Caustics and Beam Steering Calculations of Negative Refractive Index Lens Antenna by the Ray Tracing Method

Phan Van Hung[1], Nguyen Quoc Dinh[1], Dang Tien Dung[2], Yoshihide Yamada[3]*

[1]*Le Quy Don Technical University,* Ha Noi-City, Viet Nam, E-mail: phanvanhung@tcu.edu.vn, dinhnq@mta.edu.vn
[2]*Telecommunications University,* Nha Trang, Viet Nam, E-mail: dangtiendungsqtt@gmail.com
[3]*Malaysia-Japan International Institute of Technology UTM,* Kuala Lumpur, Malaysia, E-mail: yoshihide@utm.my
* Correspondence: Nguyen Quoc Dinh (dinhnq@mta.edu.vn)

***Abstract*—A negative refractive index lens antenna has a high direction, a capacity to produce multiple beams and beam steering with a thin antenna size. These characteristics enable the lens antenna to be chosen as one of the effective antennas for the base station antenna in mobile communications, meeting the rapid growth in wireless connections. In this paper, the authors use a ray tracing method to calculate and determine the caustic points and their trajectories for a negative refractive index lens. These caustic points are the feed-setting positions from which the antenna can generate the beams at the desired angles. The authors also perform the simulations of negative refractive index lens antennas with feed horns set at caustics and reference feed points. The results show the accuracy and efficiency of the calculation of caustic points and the beam steering ability of the lens antennas with negative refractive indexes.**

Keywords—Negative refractive index, lens antenna, ray tracing, caustics, beam steering

I. INTRODUCTION

The recent years have witnessed revolutionary advances in information and communication. The continuous introduction of mobile communication networks from 1G to 5G has exerted a powerful influence on all aspects of our life, from health and transportation to economy. The rapid increase in wirelessly connected devices requires an antenna system at a base station to have the ability to produce multiple beams and steer the beams in order to accommodate multiple wireless connections at the same time in different locations [1]-[5]. In 5G mobile communications, in the 28 GHz band, a lens antenna is considered a potential candidate [6], [7]. In the lens antenna design and electrical performance simulation, the ray tracing method is mainly used [8]-[15]. Off-focus feed settings suitable for wider beam steering are determined based on the convergent rays using the ray tracing method in the receiving mode. The calculation of caustic points employing the ray tracing method was studied and applied to lens antennas with positive refractive indexes [8]-[10], [12], [14]. However, studies have yet to carry out the calculations of caustic points and the simulation of wider beam steering as to lens antennas with negative refractive indexes by adopting the ray tracing method. Therefore, the authors use this method to determine the caustic points and trajectories of those points and perform the electromagnetic field simulation to consider the beams steering possibility of the negative refractive index lens antennas.

The paper is structured into five parts. Part 2 presents the basic structure of lens antennas. The algorithms and ray tracing equations are illustrated in Part 3. The structures of beam steering and beam steering radiation patterns are shown in Part 4. The conclusion is summarized in Part 5.

II. ANTENNA CONFIGURATION

The antenna structure consists of a lens with a negative refractive index and a feed element in the coordinate system, shown in Figure 1. The lens has a circular structure rotating around the oz axis. Oz is also the radiation direction of the lens antenna [6], [12], [16]. The lens has a focal point located at the origin of the coordinate system, with the distance F from the focal point to the lens vertex.

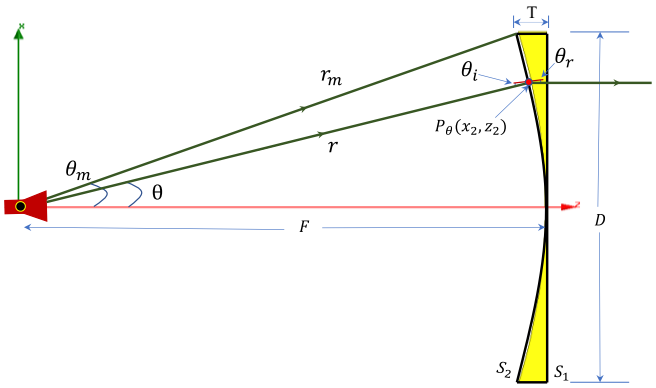

Fig. 1. The lens antenna structure.

During the operation, the rays radiated from the feed element reach the inner curved lens surface at a point expressed by P_θ, whose coordinates are (x_2, z_2), where θ is the radiation angle, from the focal point to the curved surface of the lens and the oz axis. The curved lens surface is determined by the equation (1) shown in [16], according to ox and oz. S_2 is the curved inner surface; S_1 is the rear planar surface of the lens. This lens antenna structure is suitable for the base station antenna in the mobile communications operating at 28GHz.

$$x = \sqrt{(n^2-1)(z-F)^2 + 2(n-1)F(z-F)} \qquad (1)$$

The above equation (1) is the equation of the inner curved lens surface in the xoz plane. The distance from the focal point to the inner surface of the lens is determined by equation (2) in polar coordinates [16], [17].

$$r = \frac{(n-1)F}{n\cos\theta - 1} \qquad (2)$$

where n is the refractive index of the lens. θ is the angle from focal point to the curved inner lens surface and the oz axis; θ_m is the maximum angle. r_m is the distance from the focal point

to the lens edge, shown in Figure 1. The lens thickness with a negative refractive index at the lens edge is given by equation (3) [16].

$$T = \left| \frac{1}{n+1} \left[\sqrt{F^2 + \frac{(n+1)F}{4(n-1)}} - F \right] \right| \tag{3}$$

θ_i and θ_r are the incident angle and the refracted angle, respectively. These angles satisfy Snell's law.

$$n = \frac{\sin\theta_i}{\sin\theta_r} \tag{4}$$

III. Focal Region Ray Tracing

A. Ray Tracing Algorithms

The flow chart of a focal region ray tracing program is shown in Figure 2. The program is built by the Matlab simulation tool. The analysis is based on the methods of calculating physical optics (OP) [8], [13]. The antenna parameters are first set such as the refractive index (n), focal length (F), the maximum angle to the edge of the lens θ_m, and the incident angle of the ray tracing from the wave plane θ_{in}. The equations of the incident ray, the refracted ray through two surfaces of the lens, the incident angle and the refractive angles are calculated on the basis of mathematical equations, physical optic conditions, and Snell's law for negative refractive index lens. This will be explained in the next part of the paper. In ray tracing method, all rays coming from the wave plane at the desired angle of the beam through the lens will be refracted through both lens surfaces. After leaving the inner curved lens surface, the rays converge at a caustic point or a focal region. When the angle of the incident rays is changed, the caustic points tend to lie on a specific trajectory [8]-[10], [13], [17]. These caustic points are the best places to set up the feed elements for the lens antenna. Accordingly, the lens antenna with multiple feed horns can produce the desired beam angle and steering beam.

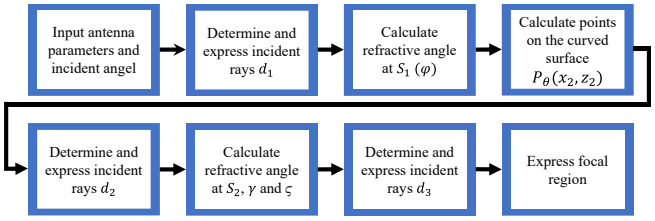

Fig. 2. Flow chart of a focal region ray tracing program.

B. Focal Regions Ray Tracing Equations

The ray tracing algorithm is calculated based on the model shown in Figure 3. With a circular lens structure rotating around the oz axis, we simply consider the wave plane perpendicular to the xoz plane; the incident rays are parallel to each other and lie on the xoz plane.

Accordingly, parallel incident rays coming from the wave plane are refracted when passing through the lens and converge in the focal region. From (2), the coordinates of P_θ, the points located on the inner curved lens surface in x-, z-direction are defined as follows $P_\theta(x_2, z_2)$:

$$\begin{aligned} x_2 &= r\sin\theta = \frac{(n-1)F\sin\theta}{n\cos\theta - 1}, \\ z_2 &= r\cos\theta = \frac{(n-1)F\cos\theta}{n\cos\theta - 1}. \end{aligned} \tag{5}$$

n_2 is a normal vector at a $P_\theta(x_2, z_2)$ on the inner curved surface S_2.

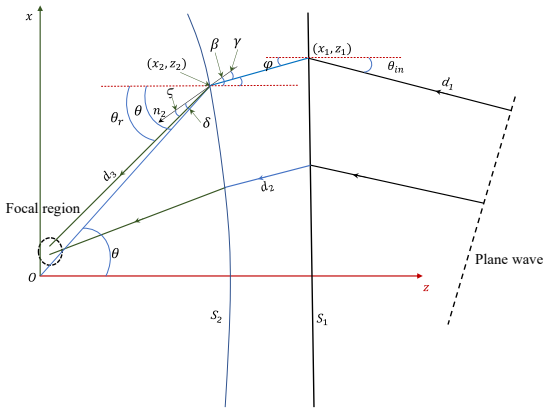

Fig. 3. Focal region in radiation mode ray tracing.

The linear equation of the incident ray (d_1) from the wave plane to the planar surface S_1 of the lens with an incident angle θ_{in} is defined as follows:

$$d_1 = \tan\theta_{in}(z - z_1) + x_1 \tag{6}$$

(i) Incident ray on S_1

According to Snell's law of refraction, the incident rays are negatively refracted, and the refracted angle of the refracted ray behind the planar surface S_1 can be determined by equation:

$$\frac{\sin\theta_{in}}{\sin\varphi} = n \tag{7}$$

$$\varphi = \arcsin\left(\frac{\sin\theta_{in}}{n}\right) \tag{8}$$

Refracted ray equation d_2 from planar surface S_1 to curved surface S_2 of the lens is given by:

$$d_2 = \tan\varphi(z - z_2) + x_2 \tag{9}$$

(ii) Incident ray on S_2

Incident angle γ of refracted ray (d_2) from planar surface S_1 to curved surface S_2 is determined based on Snell's law of refraction for original ray:

$$\frac{\sin\delta}{\sin\beta} = n \tag{10}$$

where $\delta = \theta - \beta$. Thus,

$$\sin(\theta - \beta) = \sin\theta\cos\beta - \cos\theta\sin\beta = n\sin\beta$$

$$\beta = \arctan\left(\frac{\sin\theta}{\cos\theta - n}\right) \quad (11)$$

Incident angle to S_2 can be written, using (8) and (11), as

$$\gamma = \beta - \varphi \quad (12)$$

(iii) Refracted ray from S_2

According to Snell's law of refraction, the refracted angle from the $P_\theta(x_2, z_2)$ on the curved surface S_2 to the caustic point is determined by

$$\frac{\sin\varsigma}{\sin\gamma} = n \quad (13)$$

$$\varsigma = \arcsin(n\sin\gamma) \quad (14)$$

From the equations (11) and (14), the angle between oz axis and the refracted ray d_3 is expressed as

$$\theta_r = \theta - (\delta - \varsigma) \quad (15)$$

(iv) Rays to caustic

From θ_r and $P_\theta(x_2, z_2)$, refracted ray equation d_3 from the curved lens surface S_2 to the caustic point is given as

$$d_3 = \tan\theta_r(z - z_2) + x_2 \quad (16)$$

Refracted rays d_3 from the curved surface S_2 based on equation (16) intersect at a point or a region, shown in Figure 3 and 4.

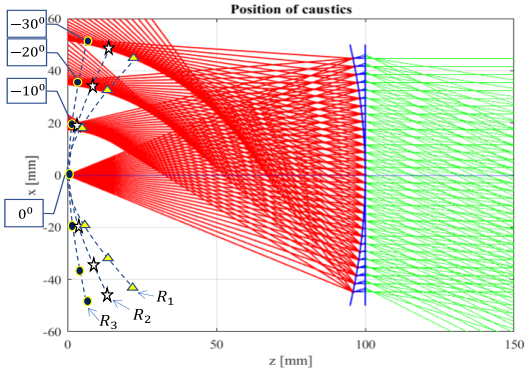

Fig. 4. Ray tracing in a focal region and caustics.

On investigation into values in the range of $\theta_{in} = \left(-30^0 \div 30^0\right)$, we obtain the focal regions. By calculating and analyzing the focal regions of the convergent points, the regions of the caustic point are limited to about two orbital arcs $R_1 = F\cos^2\alpha$ and $R_3 = F$, where α is the angle formed by the incident ray from the caustic point to the lens vertex and the oz axis, as shown in Figure 5.

IV. Beam Steering Characteristics

A. Beam Steering Modeling

Figure 5 shows the simulation structure of the lens antenna. The lens has a negative refractive index. The relative permittivity and relative permeability of the lens are $\varepsilon_r = -2$ and $\mu_r = -1$, respectively. The curved lens surface is set according to equation (2), and the lens has a circular structure that rotates around the oz axis. The focal point of the lens is on the origin of the coordinate system. The focal length is 100 millimeters from the focal point to the lens vertex. The diameter of the lens is *D*. The ratio $F/D = 1$. The conical horn antennas are set to be the wide-angle radiation for the lens. To investigate the wider beam steering feature of the negative refractive index lens antenna, the authors set up the conical horn antennas at the caustic points on the proposed trajectories (R_1, R_2, R_3, R_4) with the angle α within the range of $\left(-30^0 \div 30^0\right)$ at a 5^0 interval, as shown in Figures 4 and 5, in which $R_2 = \frac{F\cos^2\alpha + F}{2}$ is the average trajectory of R_1 and R_3 ; and $R_4 = \frac{F}{\cos\alpha}$ is the trajectory where the considered points are on the ox axis. The conical horn antenna is designed to operate at 28 GHz and reaches a maximum gain of 15.15 dBi. The caustic point is located at the horn throat, which intersects the waveguide and the horn flare.

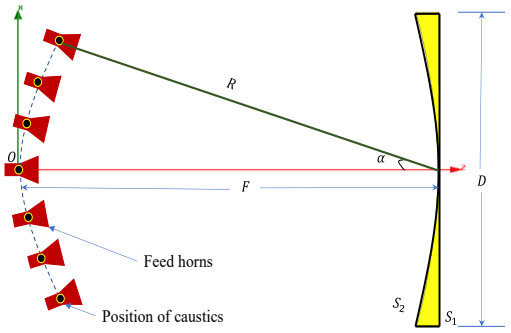

Fig. 5. A lens antenna structure with multiple feed horns.

Beam Steering Characteristics

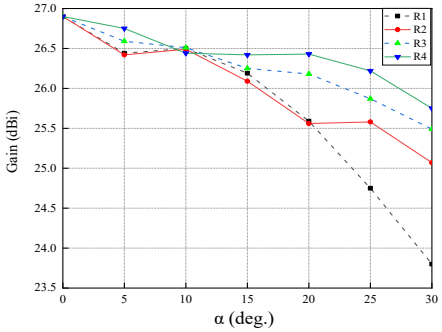

Fig. 6. The comparison of gain change at the angle α.

Figure 6 shows the variation of gain values when changing the radiation angles of the feed horn on the proposed trajectories. The results show that gain max peaks at 26.90 dBi when the feed horn is set at the origin (focal point). This value gradually decreases when the feed horn is located at the ascending angle α. The gain change occurs the most when the feed point is set on the R_1 trajectory, reducing from 26.90 dBi at 0^0 to 23.80 dBi at 30^0. When the feed horn is on the trajectory R_3 at 30^0 angle, the gain of the lens antenna drops only by 1.41 dBi, compared to its gain when setting up the feed horn at 0^0.

In Figure 7, it is clearly observed that at 5^0, the SLL reaches the lowest value of -22.95 dB when the feed horn is

set on trajectories R_3 and R_4. When the feed horn is set on trajectory R_1, the farther from the focal point the feed horn is, the faster the SLL increases. At 25^0 and 30^0, SLL are -17.73 dB and -17.13 dB, respectively. Meanwhile, the SLL of the lens antenna is still lower than -19.24 dB when located at all angles on trajectories R_2 and R_3. Besides, the authors place feed horns on the ox axis (R_4) with the respective angles and find that although the gain is maintained at a level higher than 25.75 dBi, the SLL is greatly increased to -17.04 dB and -14.59 dB at 25^0 and 30^0. Based on the calculation and simulation results above, it is possible to select suitable locations to set the feed horn so as to achieve a high gain and a low SLL.

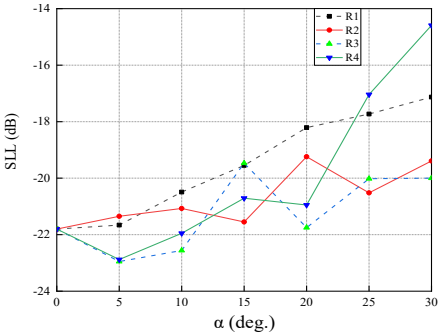

Fig. 7. The comparison of the side lobe levels at angles α.

Figure 8 shows the radiation pattern of the lens antenna with feed points placed on trajectory R_2 with the radiation angles α in the range $\left(-30^0 \div 30^0\right)$ at a 5^0 interval. It is clearly seen that the antenna radiation pattern is relatively uniform. Gain values are always maintained above 25.07 dBi. The difference in gain values when the feed horn is set at $\alpha = 30^0$ and $\alpha = 0^0$ is 1.83 dBi. SLL is maintained at less than -19.24 dB. Thus, setting the feed horn on trajectories and defined angles allows the negative refractive index lens antenna to produce multiple beams and beam steering at desired angles.

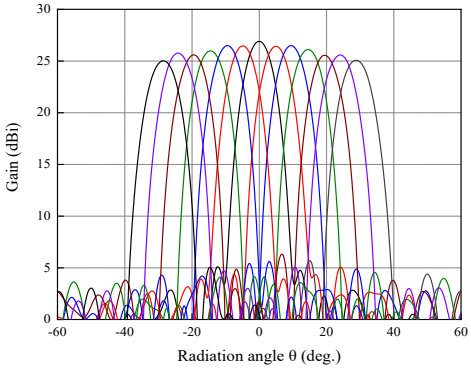

Fig. 8. Beam steering results on trajectory R_2.

V. Conclusions

By using the ray tracing method and antenna structure simulation by MATLAB tool and ANSYS HFSS electromagnetic field software, in this paper, the authors have calculated and determined relative caustics and trajectories for the negative refractive index lens antennas. The results show the effectiveness of the feed horn setup. The feed horns at the caustic points are calculated to show the beam steering ability of the negative refractive index lens antennas. The results of the research will serve as a basis for applying a multi-beam lens antenna design to the base station in 5G mobile communications.

Acknowledgment

This research is funded by Vietnam National Foundation for Science and Technology Development (NAFOSTED) under grant number 102.04-2018.08.

References

[1] W. Hong, H.Z. Jiang, C. Yu, J. Chao, P. Cheng, "Multibeam Antenna Technologies for 5G Wireless Communications," IEEE Trans. Antennas Propag., vol. 65, no. 12, pp. 6231-6249, Dec. 2017.

[2] C.X. Wang, F. Haider, X. Gao, X.H. You, Y. Yang, "Cellular architecture and key technologies for 5G wireless communication networks," IEEE Commun. Mag., vol. 52, no. 2, pp. 122-130, 2014.

[3] C.C. Chang, R.-H. Lee, and T.-Y. Shih, "Design of a Beam Switching/Steering Butler Matrix for Phased Array System," IEEE Trans. Antennas Propag., vol. 58, no. 2, pp. 367-374, Feb. 2010.

[4] Y. Yamada, C.Z. Jing, N.H.A. Rahman, K. Kamardin, I.I. Idrus, M. Rehan, T.A. Latef, T.A. Rahman, N.Q. Dinh, "Unequally Element Spacing Array Antenna with Butler Matrix Feed for 5G Mobile Base Station," In 2nd International Conference on Telematics and Future Generation Networks (TAFGEN), Kuching, Malaysia, 24-26 July 2018, pp. 72-76.

[5] N.Q. Dinh, N.T. Binh, Y. Yamada, N. Michishita, "The Density Tapering Concept of An Unequally Spaced Array by Electric Field Distributions of Electromagnetic Simulations," Journal of Electromagnetic Waves and Applications, vol. 34, no. 5, pp. 668-681. 2020.

[6] P.V. Hung, N.Q. Dinh, T.V.D. Nguyen, Y. Yamada, N. Michishita, and M.T. Islam, "Electromagnetic Simulation Method of a Negative Refractive Index Lens Antenna," in 2019 International Conference on Advanced Technologies for Communications (ATC), Hanoi, Vietnam, Oct. 2019, pp. 109-112.

[7] P.V. Hung, N.Q. Dinh, H.T. Thuyen, N.T. Hung, L.M. Thuy, L.T. Trung, and Y. Yamada, "Estimations of Matching Layers Effects on Lens Antenna Characteristics", EAI INISCOM 2020 - 6th EAI International Conference on Industrial Networks and Intelligent System,Virtual Space, 27-28 August 2020.

[8] F. Ansarudin, T. A. Rahman, and Y. Yamada, "MATLAB Program for Dielectric Lens Antenna Shaping," in 2018 2nd International Conference on Telematics and Future Generation Networks (TAFGEN), Kuching, Malaysia, Jul. 2018, pp. 81-86.

[9] Y. Tajima, Y. Yamada, S. Sasaki, and A. Kezuka, "Calculation of Wide Angle Radiation Patterns and Caustics of a Dielectric Lens Antenna by a Ray Tracing Method," IEICE Trans. Electron., vol. E87-C, no. 9, pp. 1432-1440, Sep. 2004.

[10] T. Maruyama, K. Yamamori, and Y. Kuwahara, "Design of Multibeam Dielectric Lens Antennas by Multiobjective Optimization," IEEE Trans. Antennas Propag., vol. 57, no. 1, pp. 57-63, Jan. 2009.

[11] N.H.A. Rahman, M.T. Islam, N. Misran, Y. Yamada, and N. Michishita, "Design of a satellite antenna for Malaysia beams by ray tracing method," in 2012 International Symposium on Antennas and Propagation (ISAP), Nagoya, Japan, Nov. 2012, pp. 1385-1388.

[12] Y. Tajima and Y. Yamada, "Design of shaped dielectric lens antenna for wide angle beam steering," Electron. Commun. Jpn. Part III Fundam. Electron. Sci., vol. 89, no. 2, pp. 1-12, 2006.

[13] NH.Abd. Rahman, M.T. Islam , N. Misran , Y. Yamada ,and N. Michishita, "Development of Ray Tracing Algorithms for Scanning Plane and Transverse Plane Analysis for Satellite Multibeam Application," Apr. 28, 2014.

[14] Y. Tajima and Y. Yamada, "Improvement of Beam Scanning Characteristics of a Dielectric Lens Antenna by Array Feeds," IEICE Transactions on Fundamentals of Electronics, Communications and Computer Sciences, Vol 7 p. 1616-1624, 2008.

[15] W.L. Stutzman and G.A. Thiele, Antenna Theory and Design. 3rd ed., John Wiley & Sons, New Jersey, US, 2012.

[16] Y.T. Lo, S.W. Lee, Antenna Handbook. 2nd ed. Van Nostrand Rainhold Company, New York (1988).

[17] T. A. Milligan, Modern Antenna Design. 2nd ed, John Wiley & Sons, New Jersey, 2005.